Journal of the Physical Society of Japan **84**, 064719 (2015)
http://dx.doi.org/10.7566/JPSJ.84.064719

Solution of Sine-Gordon Equations with Weak and Moderate Inductive Couplings under Bias Current and Dissipations

Feng Liu[1,2] and Xiao Hu[1,2*]

[1]*International Center for Materials Nanoarchitectonics (WPI-MANA), National Institute for Materials Science, Tsukuba, Ibaraki 305-0044, Japan*
[2]*Graduate School of Pure and Applied Sciences, University of Tsukuba, Tsukuba, Ibaraki 305-8571, Japan*

(Received April 1, 2015; accepted April 23, 2015; published online June 1, 2015)

It is found that coherent electromagnetic (EM) radiation in terahertz (THz) band takes place when a single crystal of cuprate high-T_c superconductor $Bi_2Sr_2CaCu_2O_{8+\delta}$ (BSCCO) is biased by a dc voltage. In this work we study the inductively coupled sine-Gordon equations which compose a good model for intrinsic Josephson junctions (IJJs) realized in BSCCO due to the strong layer structure. We derive a general solution for the coupled sine-Gordon equations valid for weak and moderate inductive couplings, which can enhance injection of dc energy into IJJs and convert it to THz EM radiation. This solution evolves into the π phase kink state known before for strong inductive coupling.

1. Introduction

The electromagnetic (EM) waves in terahertz (THz) range have various applications such as imaging, radar, safety checks, and so on.[1,2] However, they are difficult to be generated by conventional electronic and photonic devices, and a compact solid-state generator of THz band is still lacking. Josephson effects can be used to excite EM wave known since its discovery,[3–7] and efforts were devoted based on array of Josephson junctions.[8–14] Intrinsic Josephson effects were observed in cuprate high-T_c superconductor $Bi_2Sr_2CaCu_2O_{8+\delta}$ (BSCCO).[15] Compared with conventional low-temperature Josephson junctions the intrinsic Josephson junctions (IJJs) have the following advantages. First the junctions are homogenous at atomic scale guaranteed by the high quality of single crystals, and secondly the superconductivity gap is large, usually of tens of meV, which in principle covers the whole range of THz band of EM wave. These merits make the IJJs fantastic candidates as source for powerful EM radiation in THz band. As a matter of fact, many experimental attempts for excitation of THz radiation from IJJs were made, for example by quasiparticle injection along the in-plane direction of BSCCO sample[16,17] and by biasing a voltage on a BSCCO sample with step-like geometry.[18] There were theoretical studies focusing on possible THz radiation from IJJs by driving Josephson vortices.[19–22] It is also proposed that the THz EM radiation can be excited by sandwiching a narrow BSCCO mesa with gold electrodes under bias voltage.[23]

An experimental breakthrough was achieved in 2007, where a THz radiation with power $\sim 1\,\mu$W was observed from a BSCCO mesa under a dc bias voltage.[24] The key experimental results are as follows: the radiation frequency and the bias voltage obey the ac Josephson relation, intense radiations are observed at frequencies of cavity resonance, and they are coherent.[24] The breakthrough raised interesting questions, such as how dc energy can be transformed into intense EM radiation compatible with cavity modes, and how a large number of junctions $\sim$600 are synchronized.

The experimental breakthrough inspired intensive discussions from both experimental and theoretical sides.[25–36] Lin and Hu investigated the phase dynamics of IJJs under bias current in terms of sine-Gordon equations with strong inductive coupling.[6,25] They proposed a novel π phase kink state, which can explain the significant experimental results mentioned above and by now has been confirmed by innumerous simulations. In the π kink state, $\pm\pi$ kinks in gauge-invariant phase difference in IJJs are developed in in-plane directions, and arrange themselves alternatingly along the c-direction. The uniform bias current and cavity modes are coupled by the π phase kink, which allows a large supercurrent flow into the system at the cavity resonances, and a part of dc energy is converted to EM radiation from the mesa edge.[6,25] Experimentally, THz radiations were observed from IJJs with cylindrical geometry[32] as discussed theoretically[27,31] and in the high bias region.[33] It is also found that the radiation power from IJJs can be enhanced by controlling the temperature distribution in the mesa sample.[34]

In this work, we derive a general solution valid for small and moderate inductive couplings and high cavity modes. It is characterized by a structure in phase difference varying in lateral directions around $\pm\pi/2$ in form of cavity mode and an alternating configuration along the c-direction similar to the π phase kink state. Compared with the π kink, the static term in phase difference of the present solution does not saturate to π and 0 at the sample edges. The present solution can enhance injection of dc energy into IJJs and covert it to THz EM radiation. This solution evolves smoothly into the π phase kink state at large inductive coupling and low cavity modes.

The remaining part of the present paper is organized as follows. In Sect. 2, we solve sine-Gordon equations with weak and moderate inductive couplings under bias current and dissipations for cavity modes $(n, 0)$ in rectangular geometry and propose its general solution. Then we calculate the current–voltage (I–V) characteristics of this solution. In Sect. 3, we discuss the relation between the present solution and the π phase kink state. In Sect. 4, we extend this solution to $(1, 1)$ cavity mode. In the discussion of Sect. 5, we compare this solution with the breather solution known for single junction. Finally, the summary is presented in Sect. 6.

2. Inductively Coupled Sine-Gordon Equations

The phase dynamics of IJJs can be described appropriately by the inductively coupled sine-Gordon equations, whose dimensionless form with driving and dissipations is given as[6]

$$\Delta\boldsymbol{\gamma} = \mathbf{M}(\sin\boldsymbol{\gamma} + \beta\partial_t\boldsymbol{\gamma} + \partial_t^2\boldsymbol{\gamma} - J_{\rm ext}\mathbf{I}), \tag{1}$$

where $(\boldsymbol{\gamma})_l = \gamma_l$ with γ_l the phase difference at the l-th junction and $\mathbf{I} = (+1, +1, +1, +1, \ldots)^{\rm T}$ the unit vector; the coupling matrix $(\mathbf{M})_{l,l-1} = (\mathbf{M})_{l,l+1} = -\zeta$, $(\mathbf{M})_{l,l} = 1 + 2\zeta$ and zero otherwise with $\zeta \equiv (\lambda_{ab}/s)^2$ the inductive coupling (λ_{ab} the penetration depth in the c-direction and s the period of IJJs lattice in c-direction); the lateral length and time are scaled by the penetration depth in the ab-plane λ_c and the inverse of intrinsic plasma frequency $\omega_{\rm c} = c/\lambda_c\sqrt{\varepsilon_c}$ (ε_c the dielectric constant of BSCCO) respectively; $\beta \equiv 4\pi\sigma_c\lambda_c/c\sqrt{\varepsilon_c}$ is the normalized c-axis conductivity of BSCCO sample and $J_{\rm ext}$ is the external current normalized by the critical current $J_{\rm c}$.

As the boundary condition in lateral directions we adopt the one for perfect magnetic conductor where the magnetic fields in lateral directions are zero at mesa edges, namely $\partial_x\boldsymbol{\gamma}(x = 0, L_x) = 0$. Because the device for exciting THz radiation is made up of a thin BSCCO mesa with thickness $L_z \sim 1\,\mu$m sandwiched by gold electrodes, the impedance is huge at the edges of junctions $Z \equiv E_z/B_y \sim \lambda/L_z$ with $\lambda \sim 300\,\mu$m the wavelength of electromagnetic fields.[23] As a reasonable approximation, we start from a closed system, and the EM radiation with small magnetic field B_y can be treated as a perturbation.[6,25] Since we are searching for states uniform in the c axis, we adopt the periodic boundary condition in this direction, noticing that the current injection has been taken into account in the present gauge of phase difference.[6,25]

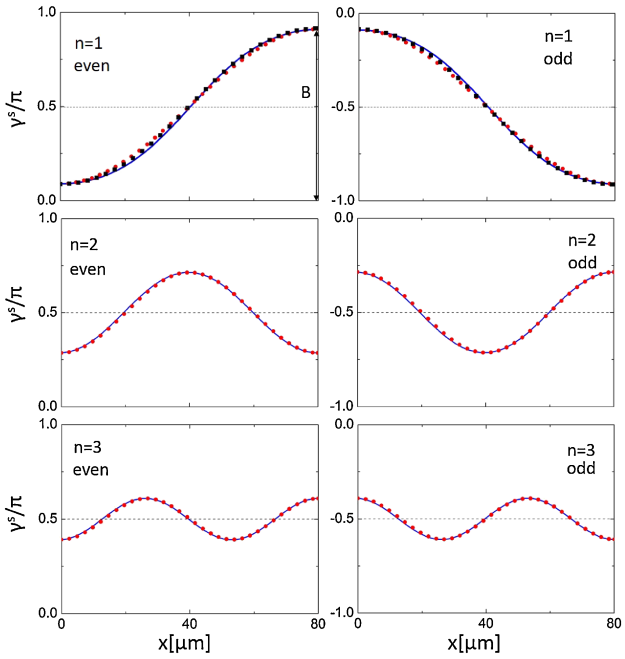

Fig. 1. (Color online) Static term γ^s in solution (2) at moderate inductive coupling and several cavity modes with left/right row for the junction with even/odd index. Red dot is the numerical result of Eq. (3) with $\zeta' = 198$, blue solid curve is the analytic solution given in Eq. (4) with $B = 0.41\pi$, 0.21π, and 0.11π for $n = 1$, 2, and 3 respectively, and black square is the simulation result of Eq. (1) with $\zeta = 230$ and $J_{\rm ext} = 0.16$ for the $(1, 0)$ cavity mode. Other parameters are taken as $\beta = 0.02$, $\lambda_c = 200\,\mu$m, $L_x = 80\,\mu$m, and $\varepsilon_c = 16$. These three solutions are in good agreement with each other and the differences among them are less than 3% in the whole space.

2.1 *General solution*

We perform computer simulation of phase dynamics in IJJs by integrating Eq. (1) with the leapfrog method.[25] Phase differences are assigned randomly between $-\pi$ and π in lateral directions and over all junctions. Under the driving of bias current, the system can be synchronized to a stable state as will be discussed in what follows. Parameters are taken as: $\zeta = 230$, $\beta = 0.02$, $\lambda_c = 200\,\mu$m, $L_x = 80\,\mu$m, $\varepsilon_c = 16$, and a current bias is taken for simulations.

Similar to the case of strong inductive coupling, the solution of Eq. (1) at small and moderate values of ζ takes the following form:[6,25]

$$\boldsymbol{\gamma}(x, t) = \left[\omega t + A\cos\left(\frac{n\pi x}{L_x}\right)\sin(\omega t + \varphi)\right]\mathbf{I} + \gamma^s(x)\mathbf{I}_2, \tag{2}$$

where the first term is the rotating phase accounting for the finite dc bias voltage according to the ac Josephson relation; the second term stands for the cavity term of the plasma oscillation with A the cavity amplitude and φ the phase shift; the last one is static, which arranges itself alternatingly along the c-direction as denoted by $\mathbf{I}_2 = (+1, -1, +1, -1, \ldots)^{\rm T}$, which is an eigen vector of coupling matrix $\mathbf{M}$: $\mathbf{M}\mathbf{I}_2 = -(4\zeta + 1)\mathbf{I}_2$.[6]

Substituting Eq. (2) into Eq. (1) and omitting higher harmonics, we obtain the following equation

$$\partial_x^2\gamma^s(x) = 2\zeta'\cos\left(\frac{n\pi x}{L_x}\right)\sin\gamma^s(x), \tag{3}$$

where $\zeta' = \zeta A\cos\varphi$. We notice that this equation is the same as that for π phase kink. The γ^s term is plotted in Fig. 1 for a moderate ζ and several typical cavity modes. We find that to a strikingly good approximation the static γ^s term can be written as

$$\gamma^s(x) = \frac{\pi}{2} - B\cos\left(\frac{n\pi x}{L_x}\right), \tag{4}$$

where B is to be determined.

Substituting the solution given in Eqs. (2) and (4) into Eq. (1) one arrives at

$$A = \frac{2J_1(B)}{\sqrt{(\beta\omega)^2 + (\omega^2 - k^2)^2}}, \tag{5}$$

$$Bk^2 = 2\zeta A\cos\varphi[J_0(B) - J_2(B)], \tag{6}$$

where $k = n\pi/L_x$ is the cavity wave number, $\tan\varphi = \beta\omega/(\omega^2 - k^2)$ and J_n is n-th Bessel function of first kind.

Figure 2 displays inductive coupling ζ and frequency ω dependencies of A and B defined in Eqs. (2) and (4) for the $(1, 0)$ cavity mode. As seen from Fig. 2, A and B grow continuously from zero at a bifurcation point of the system. Below this point, the system takes the McCumber state.[6]

2.2 *I–V characteristics*

Simultaneously with Eqs. (5) and (6) one obtains the external current[6,25]

$$J_{\rm ext} = \beta\omega + \frac{A\sin\varphi}{2L_x}\int_0^{L_x}\cos(kx)\cos\gamma^s\,dx. \tag{7}$$

It is clear that the cavity mode and the uniform external current are coupled by the γ^s term, a scheme similar to the π kink state. The I–V characteristics of the present solution is plotted in Fig. 3 for $\zeta = 230$, where large supercurrent flows

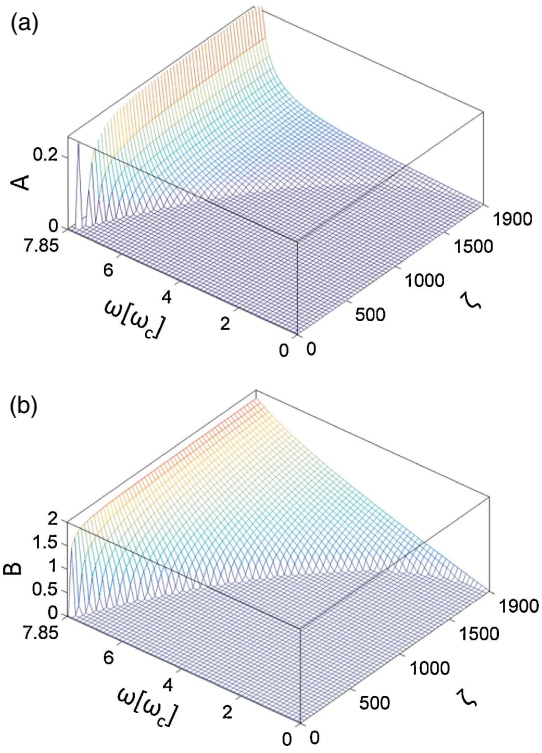

Fig. 2. (Color online) (a) and (b): inductive coupling ζ and frequency ω dependencies of A and B defined in Eqs. (2) and (4) for the $(1,0)$ cavity mode. Parameters are taken same as those for Fig. 1.

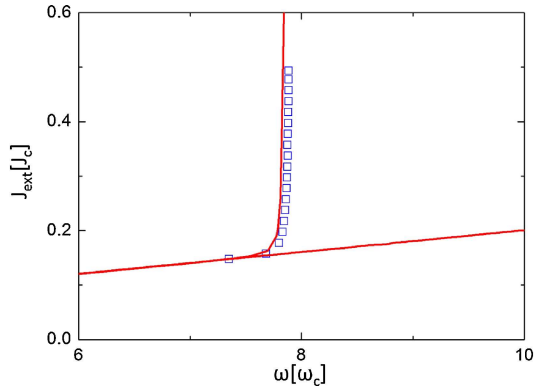

Fig. 3. (Color online) I–V characteristics of the $(1,0)$ cavity mode for $\zeta = 230$. Solid curve represents the analytic result of Eqs. (5) to (7) and square is the simulation result of Eq. (1). Other parameters are taken same as those for Fig. 1.

into the system at the resonance voltage of $(1,0)$ cavity mode $\omega_{\rm cav} = 7.85$ which corresponds to 1.2 mV. Thus, this solution is expected to be useful for the realization of powerful radiation. The detailed shape of I–V characteristics does not depend on ζ sensitively.

3. Relation with the π Phase Kink State

As the present solution and the π phase kink state share many similarities, one may naturally ask the relationship between them. To understand this, we estimate the typical length of the π phase kink. From Eq. (3) the typical length of the π phase kink can be obtained as

$$\lambda_\pi = \left(2\zeta' \frac{n\pi}{L_x}\right)^{-1/3}. \tag{8}$$

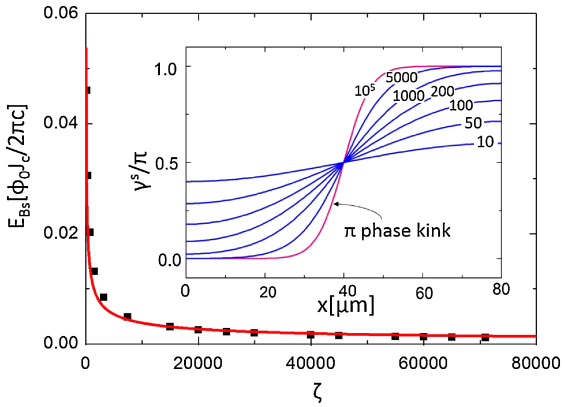

Fig. 4. (Color online) Inductive coupling ζ dependence of static magnetic energy E_{B_s} obtained by the simulation on Eq. (1) at $J_{\rm ext} = 0.4$. The red curve is for $E_{B_s} \sim 1/\sqrt{\zeta}$. The inset shows the evolution process of the present solution to the π phase kink state when the inductive coupling ζ increases obtained by the simulation of Eq. (1). Other parameters are taken same as those for Fig. 1.

The lateral size of IJJs cannot contain enough π kinks for the corresponding cavity mode when $n\pi\lambda_\pi > L_x$. Rewriting this condition in terms of ζ' and n based on Eq. (8):

$$2\zeta' < \left(\frac{n\pi}{L_x}\right)^2, \tag{9}$$

it becomes clear that when the inductive coupling is small and/or the cavity mode is high, the π phase kink state becomes unstable. In this case the π phase kink state deforms into the present solution, where the static phase term does not reach π and 0 at sample edges.

We plot in Fig. 4 the magnetic energy per junction $E_{B_s} = \langle \partial_x \boldsymbol{\gamma}^{sT} \mathbf{M}^{-1} \boldsymbol{\gamma}^s \rangle_x / N$ with $\boldsymbol{\gamma}^s = \gamma^s \mathbf{I}_2$ and N the number of junctions for ζ ranging from 10 to 10^5. One sees that the static magnetic energy is $E_{B_s} \sim 1/\sqrt{\zeta}$ in the whole range of ζ, which suggests that the present solution continuously evolves into the π phase kink state as ζ increases. As a matter of fact, when the inductive coupling ζ increases from 10 to 10^5, the γ^s term evolves into the π phase kink gradually as seen in the inset of Fig. 4.

4. Other Cavity Modes

So far we concentrate on $(1,0)$ cavity mode. One can extend the discussion to other cavity modes. Here we show $(1,1)$ mode in a rectangular mesa as an example. Based on simulation on Eq. (1), the γ^s term for $(1,1)$ cavity mode can be written as

$$\gamma^s(x,y) = \frac{\pi}{2} - B\cos\left(\frac{\pi x}{L_x}\right)\cos\left(\frac{\pi y}{L_y}\right), \tag{10}$$

where L_y is the mesa size in y-direction. The term $\gamma^s(x,y)$ and I–V characteristics of the $(1,1)$ mode are displayed in Fig. 5. For clarity we only show the simulation result of Eq. (1) for $\zeta = 230$ and $J_{\rm ext} = 0.19$, noticing that the differences among simulation result of Eq. (1), numerical solution of Eq. (3) for $\zeta' = 198$ and the analytic solution Eq. (10) with $B = 0.46\pi$ are less than 5% in the whole space.

5. Discussion

Krasnov studied the phase dynamics of IJJs especially for high cavity modes and discussed that a breather-like solution

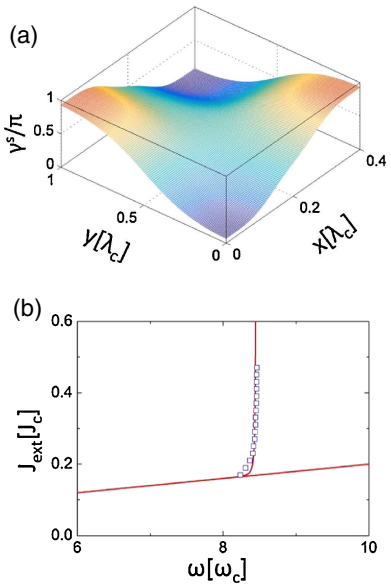

Fig. 5. (Color online) (a): spatial distribution of γ^s term for $(1,1)$ cavity mode given by the simulation on Eq. (1) for $J_{\rm ext} = 0.19$; (b): I–V characteristics of the $(1,1)$ cavity mode. Solid curve represents the analytic result of Eqs. (5) to (7) and square is the simulation result of Eq. (1). Here $\zeta = 230$, $L_y = 200\,\mu$m, and other parameters are taken same as those for Fig. 1.

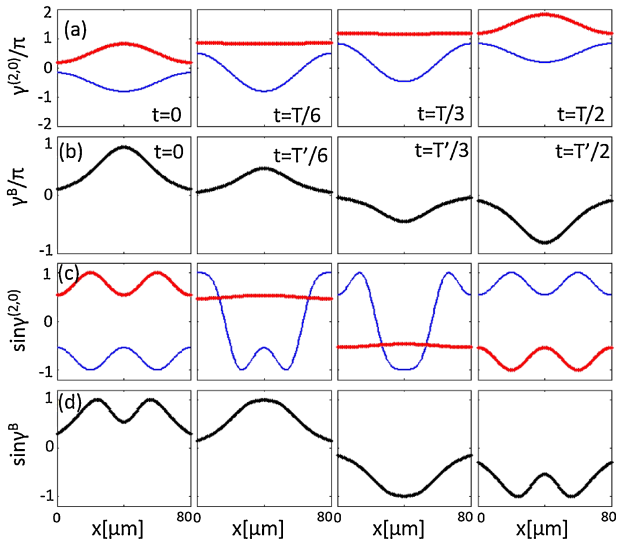

Fig. 6. (Color online) (a) and (b): Snapshots of time evolution of the present solution for $(2,0)$ cavity mode and breather solution in a half period respectively, the red/blue (thick/thin) curve represents the junction with even/odd index in the c-direction; (c) and (d): snapshots of time evolution of $\sin\gamma$ for $(2,0)$ cavity mode and $\sin\gamma^B$ respectively in a half period. Here $T = 2\pi/\omega$ with $\omega = 15.7$ and $T' = 2\pi/\omega'$ with $\omega' = 0.8$.

may be stabilized.[37] Here we discuss the relation between the present solution and the breather solution[38]

$$\gamma^B(x,t) = 4\mathrm{atan}\left[\frac{\sqrt{1-\omega'^2}\cos\omega' t}{\omega'\cosh(\sqrt{1-\omega'^2}x)}\right] \qquad (11)$$

with $\omega' \leq 1$. Compared with the present solution discussed above, first we notice that the frequency ω' in breather solution has a different meaning, which is determined by the eigen values of related inverse scattering problems to the sine-Gordon equation,[38] and not directly related to the applied voltage like ω in the present solution. Secondly the peak value of the breather solution becomes smaller when ω' is approaching unity, while in the present solution both the amplitudes of cavity mode and static term become larger when ω is closer to the resonance one. The snapshots of time evolution of present solution $\gamma(x,t)$ for $(2,0)$ cavity mode, $\gamma^B(x,t)$, $\sin\gamma$ and $\sin\gamma^B$ are shown in Fig. 6 in half period. To make the comparison apparent, we set the maximal value of breather solution similar to the one of present solution for $(2,0)$ cavity mode near resonance by choosing $\omega' = 0.8$ in Fig. 6. As seen in Figs. 6(a) and 6(b), although the even branch of present solution and breather solution have a similar shape at $t = 0$, they become different during the time evolution, for example the even branch of present solution becomes flat at $t = T/6$ and $t = T/3$ while the shape of breather solution remains domed at $t = T'/6$ and $t = T'/3$. For the supercurrent distributions of the present solution and breather solution displayed in Figs. 6(c) and 6(d), we can see that although the supercurrent of breather solution has a similar shape to the supercurrent of even branch of the present solution at $t = 0$ and $t = T/2$ ($t = T'/2$), their time evolutions are different. According to our study, what was seen in simulations by Krasnov[37] is actually the solution revealed in the present work.

6. Summary

We solve coupled sine-Gordon equations with weak and moderate inductive couplings under current driving and dissipations for the phase dynamics of intrinsic Josephson junctions. We find a general solution characterized by a static term γ^s in gauge-invariant phase differences in intrinsic Josephson junctions, which is distributed around $\pm\pi/2$ in form of cavity mode in in-plane directions and arranged alternatingly along c-direction. This solution is stable at small and moderate inductive couplings and high cavity modes, and evolves into the π phase kink state at large inductive coupling. Calculating the I–V characteristics of this solution, we show that large energy can be pumped into the cavity modes at the resonance voltages, which is useful for strong terahertz electromagnetic radiation.

Acknowledgements

The authors want to thank V. M. Krasnov and S.-Z. Lin for useful discussions. This work was supported by WPI Initiative on Materials Nanoarchitronics, MEXT, Japan.

*HU.Xiao@nims.go.jp

1) B. Ferguson and X.-C. Zhang, Nat. Mater. **1**, 26 (2002).
2) M. Tonouchi, Nat. Photonics **1**, 97 (2007).
3) B. D. Josephson, Phys. Lett. **1**, 251 (1962).
4) B. D. Josephson, Rev. Mod. Phys. **36**, 216 (1964).
5) P. W. Anderson and J. M. Rowell, Phys. Rev. Lett. **10**, 230 (1963).
6) X. Hu and S.-Z. Lin, Supercond. Sci. Technol. **23**, 053001 (2010).
7) U. Welp, K. Kadowaki, and R. Kleiner, Nat. Photonics **7**, 702 (2013).
8) T. Finnegan and S. Wahlsten, Appl. Phys. Lett. **21**, 541 (1972).
9) N. F. Pedersen, O. H. Soerensen, J. Mygind, P. E. Lindelof, M. T. Levinsen, and T. D. Clark, Appl. Phys. Lett. **28**, 562 (1976).
10) A. K. Jain, K. K. Likharev, J. E. Lukens, and J. E. Sauvageau, Phys. Rep. **109**, 309 (1984).
11) A. V. Ustinov, H. Kohlstedt, M. Cirillo, N. F. Pedersen, G. Hallmanns, and C. Heiden, Phys. Rev. B **48**, 10614 (1993).

12) K. Wiesenfeld, S. P. Benz, and P. A. A. Booi, J. Appl. Phys. **76**, 3835 (1994).
13) M. Darula, T. Doderer, and S. Beuven, Supercond. Sci. Technol. **12**, R1 (1999).
14) P. Barbara, A. B. Cawthorne, S. V. Shitov, and C. J. Lobb, Phys. Rev. Lett. **82**, 1963 (1999).
15) R. Kleiner, F. Steinmeyer, G. Kunkel, and P. Müller, Phys. Rev. Lett. **68**, 2394 (1992).
16) E. Kume, I. Iguchi, and H. Takahashi, Appl. Phys. Lett. **75**, 2809 (1999).
17) K. Lee, W. Wang, I. Iguchi, M. Tachiki, K. Hirata, and T. Mochiku, Phys. Rev. B **61**, 3616 (2000).
18) I. E. Batov, X. Y. Jin, S. V. Shitov, Y. Koval, P. Müller, and A. V. Ustinov, Appl. Phys. Lett. **88**, 262504 (2006).
19) S. Sakai, P. Bodin, and N. F. Pedersen, J. Appl. Phys. **73**, 2411 (1993).
20) M. Tachiki, T. Koyama, and S. Takahashi, Phys. Rev. B **50**, 7065 (1994).
21) R. Kleiner, T. Gaber, and G. Hechtfischer, Phys. Rev. B **62**, 4086 (2000).
22) S.-Z. Lin, X. Hu, and M. Tachiki, Phys. Rev. B **77**, 014507 (2008).
23) L. N. Bulaevskii and A. E. Koshelev, Phys. Rev. Lett. **99**, 057002 (2007).
24) L. Ozyuzer, A. E. Koshelev, C. Kurter, N. Gopalsami, Q. Li, M. Tachiki, K. Kadowaki, T. Yamamoto, H. Minami, H. Yamaguchi, T. Tachiki, K. E. Gray, W.-K. Kwok, and U. Welp, Science **318**, 1291 (2007).
25) S.-Z. Lin and X. Hu, Phys. Rev. Lett. **100**, 247006 (2008).
26) A. E. Koshelev and L. N. Bulaevskii, Phys. Rev. B **77**, 014530 (2008).
27) X. Hu and S.-Z. Lin, Phys. Rev. B **78**, 134510 (2008).
28) A. E. Koshelev, Phys. Rev. B **78**, 174509 (2008).
29) S.-Z. Lin and X. Hu, Phys. Rev. B **79**, 104507 (2009).
30) T. Koyama, H. Matsumoto, M. Machida, and K. Kadowaki, Phys. Rev. B **79**, 104522 (2009).
31) X. Hu and S.-Z. Lin, Phys. Rev. B **80**, 064516 (2009).
32) M. Tsujimoto, K. Yamaki, K. Deguchi, T. Yamamoto, T. Kashiwagi, H. Minami, M. Tachiki, K. Kadowaki, and R. A. Klemm, Phys. Rev. Lett. **105**, 037005 (2010).
33) H. B. Wang, S. Guénon, B. Gross, J. Yuan, Z. G. Jiang, Y. Y. Zhong, M. Grunzweig, A. Iishi, P. H. Wu, T. Hatano, D. Koelle, and R. Kleiner, Phys. Rev. Lett. **105**, 057002 (2010).
34) I. Kakeya, Y. Omukai, T. Yamomoto, K. Kadowaki, and M. Suzuki, Appl. Phys. Lett. **100**, 242603 (2012).
35) F. Liu, S.-Z. Lin, and X. Hu, Supercond. Sci. Technol. **26**, 025003 (2013).
36) F. Liu and X. Hu, to be published in Int. J. Mod. Phys. B.
37) V. M. Krasnov, Phys. Rev. B **83**, 174517 (2011).
38) M. J. Ablowitz, A. C. Newell, and H. Segur, Phys. Rev. Lett. **30**, 1262 (1973).